

Microwave Photonic Bistatic Radar for Real-Time and High-Resolution Imaging

Beichen Fan, Fangzheng Zhang¹, Senior Member, IEEE, Cong Ma¹, Yue Yang, Shilong Pan¹, Senior Member, IEEE, and Xiangchuan Wang¹

Abstract—A microwave photonic bistatic radar system with spatially separated transmitter and receiver is proposed. The transmitter generates a broadband linear frequency modulated (LFM) signal with the assistance of photonic frequency multiplication technique, and the radar echoes are de-chirped with photonic balanced in-phase and quadrature (I/Q) de-chirping technique in the receiver. The reference optical signal is transferred from the transmitter to the receiver by optical fiber. Experimentally, a K-band microwave photonic bistatic radar with an instantaneous bandwidth of 8 GHz is demonstrated. A set of contrast experiments are also carried out to verify the feasibility of the proposed system. Furthermore, a bistatic inverse synthetic aperture radar (ISAR) imaging experiment is conducted to confirm the real-time and high-resolution imaging capability of the proposed radar system.

Index Terms—Microwave photonics, bistatic radar, balanced I/Q de-chirping, ISAR imaging.

I. INTRODUCTION

MICROWAVE photonic radar has attracted lots of attention, which uses photonic technologies to generate and process radar signals [1]–[6]. In the transmitter of a microwave photonic radar, broadband radar signal can be generated by frequency up-conversion with a mode-locked-laser (MLL) [1], optical chirp to microwave chirp conversion using dispersive fiber [2], photonic digital to analog conversion [3], photonic frequency multiplication [4], [5], or the period-one dynamics of optically injected semiconductor laser [6]. In the receiver, the broadband radar echoes can be sampled by photonic analog-to-digital conversion (ADC) realized by optical pulse sampling [1] and temporal stretching [2], or de-chirped by photonic frequency mixing [4], [5]. Thanks to the broadband operation capability of photonic technologies, microwave photonic radars can have an ultra-high range resolution, which is particularly favorable for high-resolution radar imaging [7], [8].

Manuscript received August 20, 2020; revised September 19, 2020; accepted September 23, 2020. Date of publication September 25, 2020; date of current version October 6, 2020. This work was supported in part by the NSFC Program under Grant 61871214, in part by the NSFC Program of Jiangsu Province under Grant BK20180066, and in part by the Jiangsu Provincial Program for High-Level Talents in Six Areas under Grant DZXX-005. (Corresponding authors: Fangzheng Zhang; Shilong Pan.)

The authors are with the Key Laboratory of Radar Imaging and Microwave Photonics, Ministry of Education, Nanjing University of Aeronautics and Astronautics, Nanjing 210016, China (e-mail: zhangfangzheng@nuaa.edu.cn; pans@nuaa.edu.cn).

Color versions of one or more of the figures in this letter are available online at <http://ieeexplore.ieee.org>.

Digital Object Identifier 10.1109/LPT.2020.3026776

Until now, most of the microwave photonic radars are demonstrated with monostatic mode. A potential problem with the microwave photonic monostatic radars is that the targets along the radar line of sight (LOS) are easily blocked when the echo signals are missed. An effective solution to this problem is using the multi-direction observation configuration with separated antennas [9]. Thanks to the low-loss transmission characteristics of optical fibers, microwave photonic technology is also considered to be a competitive solution for distributed radar networks. Recently, a few microwave photonic distributed radar systems have been proposed [10], [11]. However, there are limitations in these systems. For example, in the microwave photonic distributed multiple-input multiple-output (MIMO) radar system proposed in [10], the bandwidth of generated signal is limited by the repetition frequency of the MLL. Besides, the radar imaging performance of moving targets is not investigated. In [11], the microwave photonic distributed coherent aperture radar uses an optical tunable delay line (OTDL) to adjust the frequency of the de-chirped signals, which can realize the coherent de-chirping reception. However, the experimental demonstration is a centralized MIMO inverse synthetic aperture radar (ISAR) imaging because the distance between the transmitting and receiving antennas is relatively small compared to the distance from the target to the antennas. In addition, the single-channel de-chirping reception would suffer from image frequency interference. In-phase and quadrature (I/Q) de-chirping can effectively solve this problem, but the receiver structure in [12] needs at least two fibers to transmit the reference signal, resulting in a complicated network if applied in distributed radar systems. Besides, limited by nonlinear electro-optical modulation efficiency, the single-sideband modulation in [12] is not suitable for high-order frequency multiplication and de-chirp processing.

In this Letter, a microwave photonic bistatic radar is proposed, of which the transmitter and receiver are separated spatially with antennas. The proposed balanced I/Q de-chirping receiver structure can simplify the fiber transmission network while transferring the reference signal. In the experiment, a microwave photonic bistatic radar with a bandwidth of 8 GHz (18–26 GHz) is built, which realizes signal generation by optical frequency quadrupling and balanced I/Q de-chirping reception. A group of contrast experiments are accomplished to verify the difference of the target detection geometrics between the bistatic radar and monostatic radar. Furthermore, bistatic ISAR imaging on multiple moving

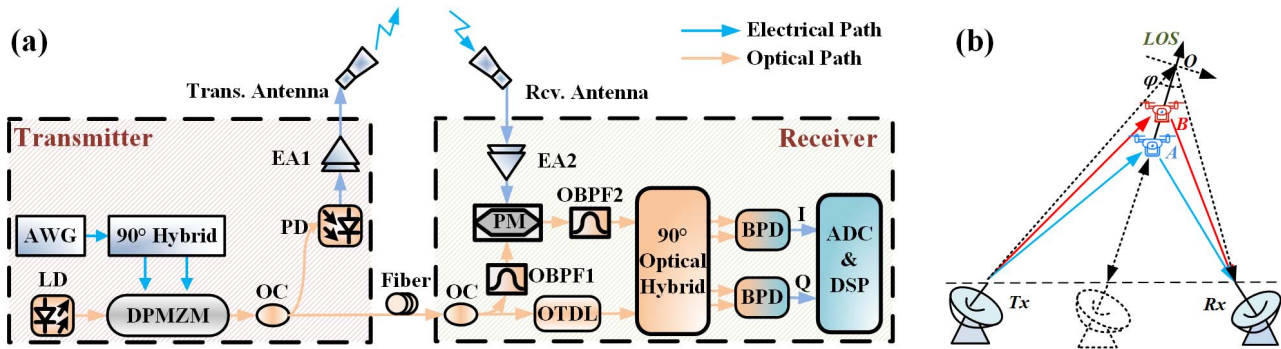


Fig. 1. (a) Schematic diagram of the microwave photonic bistatic radar and (b) geometry of target detection by a bistatic radar. LD: laser diode; AWG: arbitrary waveform generator; DPMZM: dual-parallel Mach-Zehnder modulator; PD: photodetector; EA: electrical amplifier; EDFA: erbium-doped fiber amplifier; OTDL: optical tunable delay line; OC: optical coupler; OBPF: optical band-pass filter; PM: phase modulator; BPD: balanced photodetector.

targets is also demonstrated to verify the real-time imaging capability of the proposed radar.

II. PRINCIPLE

Fig. 1(a) shows the schematic diagram of the proposed microwave photonic bistatic radar. In the transmitter, a continuous-wave (CW) light from a laser diode (LD) is modulated by a dual-parallel Mach-Zehnder modulator (DPMZM), which is driven by two intermediate frequency linear frequency modulated (IF-LFM) signals with 90° phase difference. When the bias voltages are properly set, the DPMZM works at frequency quadrupling mode, generating the $\pm 2^{\text{nd}}$ -order modulation sidebands [13]. The obtained optical signal is divided into two branches after an optical coupler (OC). The signal in the upper branch is sent to a photodetector (PD) to complete the optical-to-electrical (O/E) conversion. A frequency-quadrupled LFM signal is obtained, which is then amplified by an electrical amplifier (EA1) and emitted to the detection area. In the lower branch, the optical signal is transmitted to the receiver through a fiber and used as the optical reference.

In the receiver, the optical reference is split into two branches by another OC. The signal in the lower branch is sent to a 90° optical hybrid through an OTDL, which is used as the optical local oscillator (LO) for de-chirping processing. Assuming τ_{TR} is the time delay of the fiber link, $\Delta\tau$ is the time delay of the OTDL, and τ_{LO} is the total time delay, i.e., $\tau_{LO} = \tau_{TR} + \Delta\tau$. The optical LO signal can be expressed as

$$e_{ref}(t) \propto J_2(m) \exp(j\omega_{opt}t - \tau_{LO}) \left\{ \begin{array}{l} \exp[j(2\omega_{RF}(t - \tau_{LO}) + 2\pi\mu(t - \tau_{LO})^2)] \\ * \left[\exp[-j(2\omega_{RF}(t - \tau_{LO}) + 2\pi\mu(t - \tau_{LO})^2)] \right] \end{array} \right\} \quad (1)$$

where J_2 is the 2^{nd} -order Bessel function, m is the modulation index, ω_{opt} is the angular frequency of the optical carrier, ω_{RF} is the angular frequency of the IF-LFM signal. Also, in Eq. (1), $-B/2\mu \leq t \leq B/2\mu$ should be satisfied, where B is the bandwidth of IF-LFM, and μ is the chirp rate of IF-LFM signal. The optical reference in the other branch is sent to an optical band-pass filter (OBPF1) to select the -2^{nd} -order modulation sideband, which is then modulated by the echo signal at an electro-optical phase modulator (PM). The echo signals can be expressed as

$$i_{echo}(t) \propto J_n^2(m) \cos(4\omega_{RF}(t - \tau) + 4\pi\mu(t - \tau)^2) \quad (2)$$

where τ is the time delay of radar echo. The OBPF2 is followed to select the $+1^{\text{st}}$ -order phase modulated sideband, which can be given as

$$e_{sig}(t) \propto j \cdot J_1(\gamma) \exp(j\omega_{opt}t - \tau_{TR}) \cdot \exp \left\{ j \left[\begin{array}{l} 2\omega_{RF}t - 4\omega_{RF}\tau + 4\pi\mu(t - \tau)^2 \\ + 2\omega_{RF}\tau_{TR} - 2\pi\mu(t - \tau_{TR})^2 \end{array} \right] \right\} \quad (3)$$

where γ is the modulation index of PM. Up to this point, the optical LO and echo-modulated signal are obtained and sent to the 90° optical hybrid. Two balanced photodetectors (BPD) are followed to perform O/E conversion. After ADC and digital signal processing, a complex digital signal can be obtained as expressed by

$$s_c = s_I(t) + js_Q(t) \propto \exp \left\{ j \left[\begin{array}{l} 8\pi\mu \left(\tau - \tau_{TR} - \frac{1}{2}\Delta\tau \right) t + 4\omega_{RF} \left(\tau - \tau_{TR} - \frac{1}{2}\Delta\tau \right) \\ - 4\pi\mu \left(\tau^2 - \tau_{TR}^2 - \tau_{TR}\Delta\tau - \frac{1}{2}\Delta\tau^2 \right) \end{array} \right] \right\} \quad (4)$$

where $S_I(t)$ and $S_Q(t)$ are the I/Q signals after the BPDs. The de-chirped frequency can be controlled within a low-frequency band by tuning the OTDL, which relaxes the requirements for high-speed BPDs and ADC. To this point, photonic I/Q de-chirping has been completed.

The geometry diagram of the microwave photonic bistatic radar is shown in Fig. 1(b), where Tx means the transmitting antenna and Rx is the receiving antenna. It can be seen intuitively that the bistatic radar with spatially separated antennas has a different observation direction compared with the monostatic radar system. This characteristic brings advantages to the station flexibility and detection stability [14], [15]. The imaging reference point O is necessary to be set as a position reference, which can be adjusted by changing the link delay in the microwave photonic ISAR system [16]. When O is further away from the radar system than the targets, the de-chirped signals of the targets actually have negative frequencies with the use of balanced I/Q de-chirping [12]. Tx , O , Rx constitute the bistatic angle ϕ . The existence of ϕ will make distortions on the distances and the Doppler frequencies of the moving targets. For example, it is well known that the frequencies of the de-chirped echo signals are determined by the positions of targets. However, in the

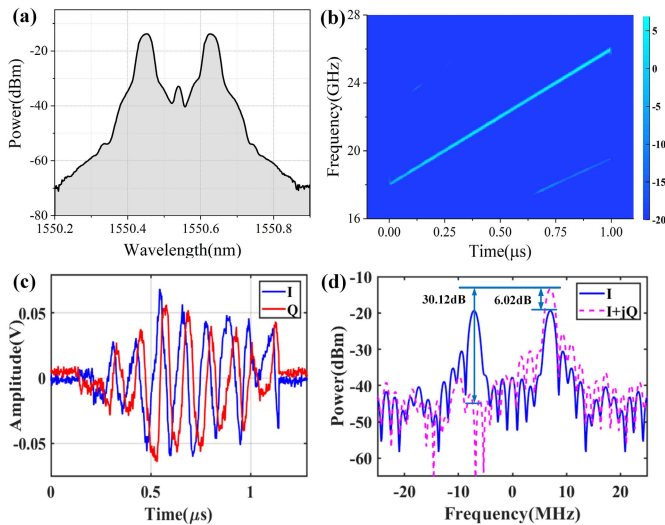


Fig. 2. (a) The optical spectrum after the DPMZM, (b) the recovered instantaneous frequency of the generated LFM signal, (c) time-domain waveforms of the de-chirped I and Q signals, (d) spectrum comparison of channel I and the complex signal $I+jQ$.

scene of bistatic ISAR imaging as shown in Fig. 1(b), the transmission paths of the target A and B will be changed due to the oblique viewing angle. The Doppler frequencies of moving targets will also change [17]. Therefore, when using the Range-Doppler algorithm to accomplish the bistatic ISAR imaging, compensations for distortions on the range motion and cross-range profile should be made in the digital signal processing [18].

III. EXPERIMENT

To verify the feasibility of the proposed radar system, an experiment is conducted. A continuous-wave light from an LD (TeraXion Inc.) is sent to a DPMZM (Fujitsu FTM7961EX). The IF-LFM signal generated by an arbitrary waveform generator (AWG, Keysight 8195A) has a bandwidth of 2 GHz (4.5~6.5 GHz), and its pulse width is 1 μ s with a duty cycle of 50%. After sent to an electrical 90° hybrid, the IF-LFM signal is transformed into two signals with 90° phase difference and then applied into the RF port. By properly setting the bias voltage of the DPMZM, the $\pm 2^{\text{nd}}$ -order sidebands are generated with the carrier suppressed, of which the spectrum is measured by an optical spectrum analyzer (YOKOGAWA AQ6370C), as shown in Fig. 2(a). After a 50:50 OC, the optical signal is split into two branches. The optical signal in one branch is sent into a 30G PD to accomplish the frequency beating. After amplified by an electrical amplifier (EA1), the generated microwave signal is emitted to the detection area by a K-band horn antenna. Fig. 2(b) shows the time-frequency diagram of the transmitted microwave signal. The optical signal in the other branch is transmitted to the receiver through fiber and used as optical reference for balanced I/Q de-chirping.

After the optical reference signal is transmitted to the receiver, it is split into two channels by a 10:90 OC. The signal in the 10% branch is sent to a 90° optical hybrid (Kylia COH28) as optical LO, while the signal in the other branch is sent to the OBPF1 (Yenista XTM-50), which selects out the -2^{nd} -order sideband as the optical carrier to be modulated by

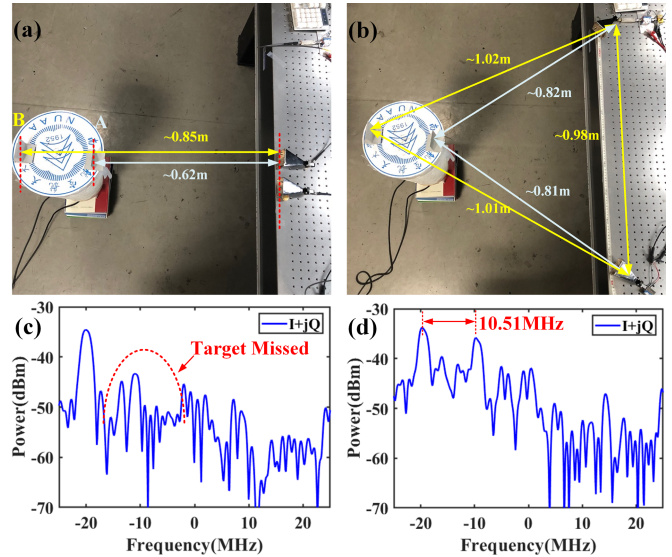


Fig. 3. Picture of the target detection with (a) monostatic radar and (b) bistatic radar, and spectrum of the de-chirped complex signal for (c) monostatic radar and (d) bistatic radar.

the echo signals at a PM (iXblue MPZ-LN-40). After received by a K-band antenna, the echoes of the corner reflector are amplified by EA2 and sent to the RF input port of the PM. After selecting the required optical frequency components by OBPF2, the echo-modulated optical signal is sent to the 90° optical hybrid to complete the photonic frequency mixing. After a pair of BPDs (Thorlabs PDB450C-AC), two de-chirped echo signals with 90° phase difference are obtained. Fig. 2(c) shows the received balanced I/Q de-chirped signals sampled by a real-time oscilloscope (Keysight DXO-X 92504a) with a 50 MSA/s sampling rate. It is shown clearly that these two signals with the same envelope have a 90° phase difference. Fig. 2(d) shows the spectra comparison of the de-chirped signal in channel I and the complex signal. As can be seen, the spectrum of the real-valued signal in single-channel has an image frequency. While, in the spectrum of complex signal, the image frequency is suppressed and the image-rejection ratio is 30.12 dB. Besides, the power of the complex signal is enhanced by 6.02 dB, compared with that of the single-channel signal.

In order to test the detection capability of the proposed radar system, a group of proportionally scaled-down mono-/bi-static radar detection experiments are performed, with the antennas placed together or separated as shown in Fig. 3(a) and 3(b). In Fig. 3(a), the transmitting and receiving antennas are placed together while the distance from the antennas to two baffle-boards (A and B) are 0.62m and 0.85m, respectively. Fig. 3(c) is the spectrum of balanced I/Q de-chirped signals, the exact target echo peak is roughly -20.09 MHz at the negative half-axis with the image frequency rejected. The reference point is at 1.07 m away from the antennas, thus there should be an echo peak between the peak of target A and zero frequency. However, due to the obstruction of target A, it is unable to receive the echo reflected from target B, which leads to target missing in the detection. But for bistatic radar, as shown in Fig. 3(b), the transmitting and receiving antennas are placed separately at a distance of 0.98 m, while the

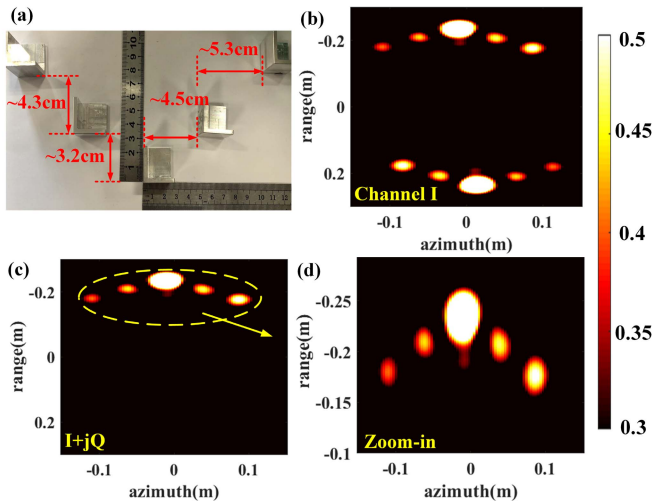


Fig. 4. (a) Picture of the imaging target, (b) bistatic ISAR image obtained by single channel de-chirping, (c) bistatic ISAR image obtained by I/Q de-chirping and (d) zoom-in view of the image with I/Q de-chirping.

positions of targets remain the same. The distances between the transmitting antenna and the receiving antenna to target A are 0.82 m and 0.81 m, to target B are 1.02 m and 1.01 m, respectively. With this configuration, the spectral peaks of the two de-chirped signals should have a frequency difference of 10.67 MHz. After compensating the de-chirped signal for the influence of the antennas' relative positions by adjusting the OTDL and processing the I/Q signals, the peak of target A is observed at the frequency of -19.89 MHz, and the peak of target B arises as expected at -9.38 MHz, as shown in Fig. 3(d). The error of the frequency difference from the theoretical value is 0.16 MHz. The measured data basically coincides with the frequency difference calculated according to the experimental scenario. Also, it can be seen that the microwave photonic radar with antennas distribution can provide a solution for detecting overlapping targets by taking advantage of the spatial information.

To verify the 2D imaging feasibility of the proposed bistatic radar, an ISAR imaging experiment for multiple moving targets is carried out. The rotator's angular velocity is set as 2π rad/s, and the targets are five corner reflectors, as shown in Fig. 4(a), in which the size of each reflector is $2.3\text{cm} \times 2.3\text{cm} \times 2.3\text{cm}$. After compensating for the influence of the bistatic angle φ , ISAR imaging using single de-chirped channel signal is shown in Fig. 4(b). It can be clearly seen that false targets generated by the imaging frequency are located symmetrically with respect to the reference point, which affects the detection accuracy of the radar system. When the I/Q signals are processed into complex signals in the digital domain, the false targets disappear and the actual targets are imaged, as shown in Fig. 4(c). It should be noted that, since the reference point is chosen beyond the corner reflectors, an inverted 'V' appears in the ISAR image. In the zoom-in view shown in Fig. 4(d), the bistatic ISAR image is clearly observed and the relative position information in the image coincides with the actual situation. Therefore, the real-time imaging feasibility of the proposed microwave photonic bistatic radar system for multiple targets is verified.

IV. CONCLUSION

In conclusion, a microwave photonic bistatic radar system with balanced I/Q de-chirping for real-time high-resolution ISAR imaging is proposed, in which the transmitter and receiver are separated and connected by a fiber link. In the experiment, by photonic generation and I/Q de-chirping of LFM signals with a bandwidth of 8 GHz, the bistatic radar can successfully distinguish two overlapping targets along the LOS of a monostatic radar and the frequency difference matches well with the calculation result. Bistatic ISAR imaging of multiple targets is carried out to further verify the real-time imaging ability to the moving targets. The proposed microwave photonic bistatic radar can be easily expanded to a distributed multistatic radar network.

REFERENCES

- [1] P. Ghelfi *et al.*, "A fully photonics-based coherent radar system," *Nature*, vol. 507, no. 7492, pp. 341–345, Mar. 2014.
- [2] W. Zou, H. Zhang, X. Long, S. Zhang, Y. Cui, and J. Chen, "All-optical central-frequency-programmable and bandwidth-tailorable radar," *Sci. Rep.*, vol. 6, Jan. 2016, Art. no. 019786.
- [3] S. Peng *et al.*, "High-resolution W-band ISAR imaging system utilizing a logic-operation-based photonic digital-to-analog converter," *Opt. Express*, vol. 26, no. 2, pp. 1978–1987, 2018.
- [4] F. Zhang, Q. Guo, and S. Pan, "Photonics-based real-time ultra-high-range-resolution radar with broadband signal generation and processing," *Sci. Rep.*, vol. 7, no. 1, p. 13848, Oct. 2017.
- [5] R. Li *et al.*, "Demonstration of a microwave photonic synthetic aperture radar based on photonic-assisted signal generation and stretch processing," *Opt. Express*, vol. 25, no. 13, pp. 14334–14340, 2017.
- [6] G. Sun, F. Zhang, and S. Pan, "Photonic-assisted high-resolution incoherent back projection synthetic aperture radar imaging," *Opt. Commun.*, vol. 466, Jul. 2020, Art. no. 125633.
- [7] F. Zhang *et al.*, "Photonics-based broadband radar for high-resolution and real-time inverse synthetic aperture imaging," *Opt. Express*, vol. 25, no. 14, pp. 16274–16281, Jul. 2017.
- [8] B. Gao, F. Zhang, E. Zhao, D. Zhang, and S. Pan, "High-resolution phased array radar imaging by photonics-based broadband digital beam-forming," *Opt. Express*, vol. 27, no. 9, pp. 13194–13203, 2019.
- [9] A. Haimovich, R. Blum, and L. Cimini, "MIMO radar with widely separated antennas," *IEEE Signal Process. Mag.*, vol. 25, no. 1, pp. 116–129, Jan. 2008.
- [10] L. Lembo *et al.*, "In-field demonstration of a photonic coherent MIMO distributed radar network," in *Proc. IEEE Radar Conf. (RadarConf)*, Apr. 2019, pp. 1–6.
- [11] X. Xiao, S. Li, S. Peng, D. Wu, X. Xue, X. Zheng, and B. Zhou, "Photonics-based wideband distributed coherent aperture radar system," *Opt. Express*, vol. 26, no. 26, pp. 33783–33796, 2018.
- [12] X. Ye, F. Zhang, Y. Yang, and S. Pan, "Photonics-based radar with balanced I/Q de-chirping for interference-suppressed high-resolution detection and imaging," *Photon. Res.*, vol. 7, no. 3, pp. 265–272, 2019.
- [13] Q. Guo, F. Zhang, P. Zhou, and S. Pan, "Dual-band LFM signal generation by optical frequency quadrupling and polarization multiplexing," *IEEE Photon. Technol. Lett.*, vol. 29, no. 16, pp. 1320–1323, Aug. 15, 2017.
- [14] M. Jackson, "The geometry of bistatic radar systems," *IEE Proc. F (Commun., Radar Signal Process.)*, vol. 133, no. 7, pp. 604–612, Dec. 1986.
- [15] E. Fishler, A. Haimovich, R. S. Blum, L. J. Cimini, D. Chizhik, and R. A. Valenzuela, "Spatial diversity in radars—Models and detection performance," *IEEE Trans. Signal Process.*, vol. 54, no. 3, pp. 823–838, Mar. 2006.
- [16] A. Wang, J. Wo, X. Luo, Y. Wang, W. Cong, P. Du, J. Zhang, B. Zhao, J. Zhang, Y. Zhu, J. Lan, and L. Yu, "Ka-band microwave photonic ultra-wideband imaging radar for capturing quantitative target information," *Opt. Express*, vol. 26, no. 16, pp. 20708–20717, 2018.
- [17] Z. Zhu, Y. Zhang, and Z. Tang, "Bistatic inverse synthetic aperture radar imaging," in *Proc. IEEE Int. Radar Conf.*, May 2005, pp. 354–358.
- [18] M. Martorella, J. Palmer, J. Homer, B. Littleton, and I. Dennis Longstaff, "On bistatic inverse synthetic aperture radar," *IEEE Trans. Aerosp. Electron. Syst.*, vol. 43, no. 3, pp. 1125–1134, Jul. 2007.